International Journal of Heat and Mass Transfer 212 (2023) 124258

Contents lists available at ScienceDirect

International Journal of Heat and Mass Transfer

journal homepage: www.elsevier.com/locate/hmt

Experimental study of the thermal probing depth of a skin calorimeter

Pedro Jesús Rodríguez de Rivera [a], Miriam Rodríguez de Rivera [b], Fabiola Socorro [a], Manuel Rodríguez de Rivera [a,*]

[a] Department of Physics, University of Las Palmas de Gran Canaria, Las Palmas de Gran Canaria, Spain
[b] Cardiology Service, Hospital Universitario Marqués de Valdecilla, Santander, Spain

ARTICLE INFO

Article history:
Received 17 January 2023
Revised 20 April 2023
Accepted 30 April 2023
Available online 17 May 2023

Keywords:
Direct calorimetry
Skin heat flux
Skin heat capacity
Skin thermal conductivity
Thermal probing depth
Thermal penetration depth

ABSTRACT

In this work we perform an experimental study of the thermal probing depth of a skin calorimeter developed to measure *in vivo* the heat capacity and the thermal resistance of a 4 cm^2 skin region. To determine these properties, a small thermal excitation is applied to the skin and then, the static and dynamic response of the calorimetric signal is studied. This excitation consists of a periodic change of the calorimeter thermostat temperature while the device is applied on the skin. We have found that the thermal penetration depth depends mainly on the period of this periodic thermal excitation. This time dependence is exponential for non-semi-infinite domains. Using a time–variant model, we performed measurements on the dorsal and volar areas of the left wrist of a healthy 64-year-old male subject. For a 4 cm^2 region of skin, the results show that the heat capacity in both zones are of the same order of magnitude. Its initial value is 4 J/K and increases exponentially up to 7 J/K with a time constant of 6.5 min. Thermal resistance also increases exponentially with time: from 27 to 36 K/W for the volar zone, and from 32 to 45 K/W for the dorsal zone.

1. Introduction

Skin is the largest organ of the human body and protects against physical impact, weather and external organisms. In its thermal regulation function, two properties are of great interest: the specific heat capacity and the thermal conductivity of the skin. Both properties characterize the transmission of heat by conduction along the skin. This phenomenon is described by the Fourier equation [1]:

$$w(t) = \rho_s c_s \frac{\partial T_s}{\partial t} + div(-\lambda_s \nabla T_s) \quad (1)$$

... where, $w(t)$ is the metabolic power generated by the skin in W/m^3, T_s is the skin tissue temperature, ρ_s its density in kg/m^3, c_s its heat capacity in J/kg·K and λ_s its thermal conductivity in W/m·K. We could add the heat provided by blood perfusion to the Fourier equation:

$$w(t) = \rho_s c_s \frac{\partial T_s}{\partial t} + div(-\lambda_s \nabla T_s) + g_b c_b (T_s - T_b) \quad (2)$$

... where, T_b is the arterial blood temperature, c_b blood specific heat capacity in J/kg·K and g_b the volumetric blood flow in $kg/s{\cdot}m^3$.

From this biothermal equation, known as the Pennes equation [2,3], several models have been developed to characterize thermal fluctuations [4], to model heat transfer in the vascular system [5], to describe the temperature distribution of skin and deeper tissues in the four extremities of the human body [6], or to analyze tissues in the presence of a tumor [7]. These equations use the skin-specific parameters ρ_s, c_s and λ_s, determined from tissue biopsy samples. Density, specific heat capacity and thermal conductivity are experimentally determined from these samples using the appropriate specific instrumentation (densimeter, calorimeters and thermal conductivity meters). As an alternative to this method, different instruments have been developed to determine these parameters on a *non-invasive* way and *in vivo*, either with contact sensors [8–10] or remotely [11,12]. In the thermoregulation processes of the human body, these properties change in every situation. Vasodilation, vasoconstriction and sweating of the skin directly affect these properties. Therefore, these *non-invasive in vivo* measurement methods are of particular interest in several applications, in particular while monitoring intense physical activities [13].

In these thermal instruments generally there is a heat source and a sensor. The working principle of these instruments consists of producing a controlled thermal perturbation and measuring its effect on the skin. To relate the thermal properties of the skin with

* Corresponding author.
E-mail address: manuel.rguezderivera@ulpgc.es (M. Rodríguez de Rivera).

https://doi.org/10.1016/j.ijheatmasstransfer.2023.124258

Nomenclature

$w\ (t)$	metabolic power generated by the skin [W/m^3]
t	time [s]
p	temperature change period [s]
T_s	skin tissue temperature [°C]
ρ_s	skin tissue density [kg/m^3]
c_s	skin tissue specific heat capacity [J/kg·K]
λ_s	skin tissue thermal conductivity [W/m·K]
T_b	arterial blood temperature [°C]
c_b	blood specific heat capacity [J/kg·K]
g_b	volumetric blood flow [kg/s·m^3]
T_1	calibration base temperature [°C]
W_1	calibration base dissipated power [W]
y	skin calorimeter calorimetric signal [V]
T_2	skin calorimeter thermostat temperature [°C]
W_2	skin calorimeter thermostat power [W]
$TF_{ij}\ (s)$	transfer function (in Laplace domain)
s	Laplace variable
K_{ij}	sensitivity of TF_{ij}, K_{1i} in [V/W] and K_{2i} in [K/W]
$\tau_1,\ \tau_2$	time constants of TF_{ij} [s]
τ^*_{ij}	opposite of the inverses of the zeros of the TF_{ij} [s]
N	model domain number
C_i	heat capacity [J/K]
C_1	... of the calibration base
C_2	of the skin calorimeter thermostat
$T_i\ (t)$	temperature of the "i" domain [°C]
P_{ik}	thermal conductance between domains 'i' and 'k' [W/K]
P_1	between C_1 and ambient
P_2	between C_2 and the cold focus
P_{12}	thermal conductance of the skin calorimeter, between C_1 and C_2
k	seebeck coefficient of the measurement thermopile [V/K]
T_{cold}	skin calorimeter cold temperature [°C]
T_{room}	ambient or room temperature [°C]
y_{exp}	experimental calorimetric signal [V]
y_{cal}	calculated calorimetric signal [V]
T_{2exp}	experimental thermostat temperature [°C]
T_{2cal}	calculated thermostat temperature [°C]
ε_y	root mean square error in the fitting of y [V]
ε_{T2}	root mean square error in the fitting of T_2 [°C]
np	number of points used in the fitting
C_{skin}	skin heat capacity [J/K]
R_{skin}	skin equivalent thermal resistance $R_{skin} = 1/P_{skin}$ [K/W]
τ_{skin}	C_{skin} and R_{skin} variation time constant [s]
t_{max}	maximum time used in the calculation of thermal properties [s]
$V_{peltier}$	Peltier element voltage supply [V]
W_{skin}	skin dissipated power [W]

the signal measured by the sensor, the equations that describe the heat transfer phenomenon (conduction, convection, and/or radiation) are used. A common problem with all these techniques is the domain considered in the skin temperature distribution. The limit of this domain will define the thermal probing depth of the instrument. The interest of thermal penetration depth extends to other applications. For example, a current research issue is how to maximize the cooling of the magnetic material in magnetocaloric cooling machines [14]. The solution proposed by some authors [8–12,14] consists of estimating the thermal penetration depth from the numerical solution of the differential Eqs. (1) and (2) mentioned above.

In this research we perform an experimental study of the thermal probing depth of a skin calorimeter designed to measure *in vivo* the heat flux and the thermal properties of the skin [15,16]. First, we describe the experimental equipment and the measurement method. Then, we describe the experimental measurements performed on human skin, and finally we summarize the conclusions of the work. The procedure applied in this study could be applied to other instruments with a similar principle of operation, even if the sensors are different. In our case the main sensor is a thermopile, in other cases it is a contact or remote temperature sensor.

2. Materials & methods

2.1. Experimental system

The skin calorimeter used in this study consists of a measuring thermopile (HOT20-65-F2A-1312 by Laird) placed between a high thermal conductivity aluminum plate that will come into contact with the skin (20 × 20 × 1 mm) and an aluminum thermostat (14 × 14 × 4 mm). On the other side of the thermostat there is a cooling system consisting of another thermopile identical to the measurement one (Peltier element), a heatsink and a fan (see diagram in Fig. 1). The thermostat temperature is measured with an RTD (Resistance Temperature Detector, 1PT100GX0518, by Omega) and is programmed using a PID control (Proportional Integrative Derivative), which determines the power to dissipate in an electrical resistor located inside the thermostat (10 Ω resistor made of constantan wire TFCC-005, by Omega). Except the heatsink and the fan, these elements are thermally insulated from the outside. A calibration base that includes an electrical resistor and a temperature sensor is used to calibrate the calorimeter. A programmable triple power supply (E3631A, by Keysight) powers the skin calorimeter's thermostat, the cooling thermopile and the calibration base resistor. A DAQ (Data Acquisition System, 34970A with 34901, by Keysight) is used to measure the calorimetric signal and the temperatures. A program written in Microsoft Visual C++ controls the instrumentation connected to a laptop *via* USB/GPIB interface (82357B, by Keysight). The sampling period in the control and data acquisition is 0.5 s.

2.2. Calorimetric model

The initial objective of this skin calorimeter was the determination of the heat flux transmitted by conduction when the calorimeter is applied on the skin. To achieve this objective, we proposed an operating model that consists of assimilating the instrument into a system with two inputs and two outputs. The inputs were the power transmitted from the skin to the skin calorimeter (W_1) and the power dissipated by the thermostat (W_2). The outputs were the calorimetric signal (y) provided by the measurement thermopile and the thermostat temperature (T_2). The linearity of the system was experimentally verified and we defined a model given by four transfer functions (in Laplace domain, where s is the Laplace variable):

$$\begin{pmatrix} Y(s) \\ T_2(s) \end{pmatrix} = \begin{pmatrix} TF_{11}(s) & TF_{12}(s) \\ TF_{21}(s) & TF_{22}(s) \end{pmatrix} \begin{pmatrix} W_1(s) \\ W_2(s) \end{pmatrix} \tag{3}$$

Thus, skin calorimeter calibration consists of determining the parameters of the transfer functions TF_{ij}. Given the signal-to-noise ratio of the measured signals, it was possible to determine a maximum of two poles. Therefore, the general form for each TF_{ij} was

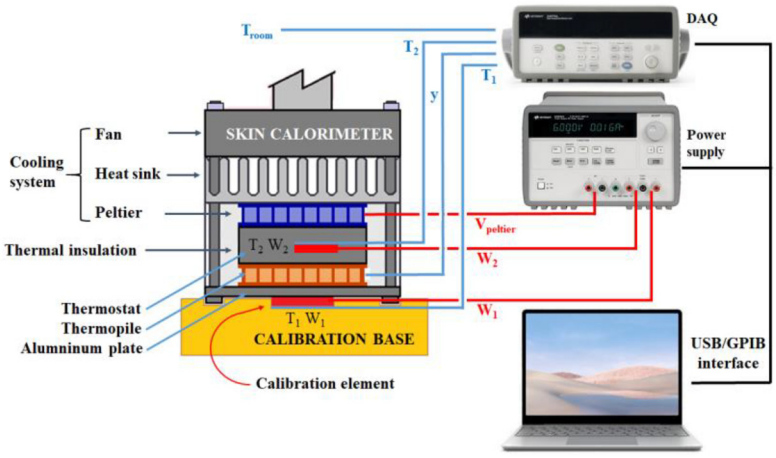

Fig. 1. Schematic of skin calorimeter & data acquisition and control system.

as follows:

$$TF_{ij}(s) = \frac{K_{ij}(1+s\tau_{ij}^*)}{(1+s\tau_1)(1+s\tau_2)} \tag{4}$$

where, K_{ij} represent the sensitivities or static gains (stationary responses to a unit step). τ_1 and τ_2 are the opposites of the inverses of the poles (time constants), and τ_{ij}^* are the opposites of the inverses of the zeros.

Later, it was found that the time constants were related with the heat capacities of the elements that composed the instrument-skin combination. Therefore, a new model widely used in the field of calorimetry [17] was proposed. This model consisted of decomposing the calorimeter into N domains of heat capacity C_i and infinite thermal conductivity, which is equivalent to assuming a temperature $T_i(t)$ in each domain. These domains are connected to each other by thermal couplings of thermal conductance P_{ik}. In the heat conduction calorimeters, the transmission by radiation is avoided, so the power developed in each domain, W_i (t), equals to the power necessary to modify its temperature plus the power transmitted by conduction to the neighboring domains:

$$W_i(t) = C_i\frac{dT_i}{dt} + \sum P_{ik}(T_i - T_k) \tag{5}$$

This system of equations allows the incorporation of fluid flow that could pass through different domains [18]. The minimum number of domains is generally given by the number of poles that can be identified. In our case, two poles can be identified, so a decomposition into two domains is enough to correctly represent the operation of the instrument. The first domain (C_1) represents the skin where the calorimeter is applied, and the second domain (C_2) represents the calorimeter thermostat. If a calibration is performed, the first domain will be the region of the calibration base where the artificial dissipation happens. The calorimetric signal provided by the measuring thermopile (y) is proportional to the difference between the temperatures of the two domains, being the constant of proportionality the Seebeck coefficient (k). The model equations are as follows:

$$\begin{aligned} W_1(t) &= C_1\frac{dT_1}{dt} + P_{12}(T_1 - T_2) + P_1(T_1 - T_{room}) \\ W_2(t) &= C_2\frac{dT_2}{dt} + P_{12}(T_2 - T_1) + P_2(T_2 - T_{cold}) \\ y(t) &= k(T_1 - T_2) \end{aligned} \tag{6}$$

Measurements must always have an initial reference or steady state, where the first derivatives of the temperatures and of the calorimetric signal are zero. This reference provides the initial baseline. We assume that during the measurement time the ambient temperature (T_{room}) and the cold temperature (T_{cold}) are constant. In addition, the thermal insulation of the calorimeter dampens possible variations in these temperatures. Correcting the baselines of all variables to this initial state, gives the following system of equations:

$$\begin{aligned} \Delta W_1(t) &= \frac{C_1}{k}\frac{d\Delta y}{dt} + \frac{P_1 + P_{12}}{k}\Delta y + C_1\frac{d\Delta T_2}{dt} + P_1\Delta T_2 \\ \Delta W_2(t) &= -\frac{P_{12}}{k}\Delta y + C_2\frac{d\Delta T_2}{dt} + P_2\Delta T_2 \end{aligned} \tag{7}$$

Applying the Laplace transform, we obtain the system of equations Eq. (8). We can see that the poles of the four transfer functions are the same. However, the sensitivities and zeros are different.

$$\begin{pmatrix} \Delta W_1 \\ \Delta W_2 \end{pmatrix} = \begin{pmatrix} \frac{C_1}{k}s + \frac{P_1+P_{12}}{k} & C_1 s + P_1 \\ -\frac{P_{12}}{k} & C_2 s + P_2 \end{pmatrix} \begin{pmatrix} \Delta Y \\ \Delta T_2 \end{pmatrix} \tag{8}$$

From this equation, we can easily determine the parameters of the four transfer functions Eqs. (3) and (4). In conclusion, the whole system *skin calorimeter - skin* can be identified with six parameters, two of them related with the skin region where the measurement is made: C_1 and P_1, and four of them specific to the skin calorimeter: C_2, P_{12}, P_2 and k.

2.3. Calibration

Calibration of the skin calorimeter consists of the determination of the calorimetric model parameters given by Eq. (8). The parameters are determined from experimental measurements in which a known power is dissipated in the calibration base [19]. The input and the output signals are known and it only remains to determine the parameters of the TF_{ij}. Fig. 2 shows an experimental measurement in which two 300 mW rectangular pulses have been programmed for 150 s at the calibration base and at the calorimeter's thermostat. This figure shows the powers (W_1 and W_2), the calorimetric signal (y) and the thermostat temperature (T_2).

To determine the model parameters, an optimization method based on the Nelder–Mead simplex algorithm [20–22] is used. The error criterion to be minimized is the Root Mean Square Error (RMSE) between the experimental curves and the curves calculated by the model:

$$\varepsilon = \alpha\varepsilon_y + \varepsilon_{T2} = \frac{\alpha}{np}\sqrt{\sum_{i=1}^{np}(\Delta y_{\exp}[i] - \Delta y_{cal}[i])^2}$$

Table 1
Identification of skin calorimeter. Model parameters when it is placed in the calibration base (C_1 represents the calibration base and C_2 the calorimeter thermostat).

Determination of heat capacities and thermal conductances Eqs. (6) and (7)		
RSME: ε_y = 12.2 μV; ε_{T2} = 1.3 mK (Eq. (9))		
	P_1 = 35.0 ± 0.6 mW/K	
C_1 = 3.56 ± 0.01 J/K	P_2 = 56.4 ± 1.3 mW/K	
C_2 = 4.29 ± 0.03 J/K	P_{12} = 113.5 ± 0.9 mW/K	k = 20.9 ± 0.01 mV/K
Sensitivities, time constants and τ_{ij}* Eqs. (3), (4) and (8)		
K_{11} = 95.40 mV/W	τ_{11}*= 76.1 s	τ_1 = 86.3 s
K_{12} = −59.20 mV/W	τ_{12}*= 101.8 s	τ_2 = 14.3 s
K_{21} = 9.20 K/W	τ_{21}*= 0 s	
K_{22} = 12.03 K/W	τ_{22}*= 24.0 s	

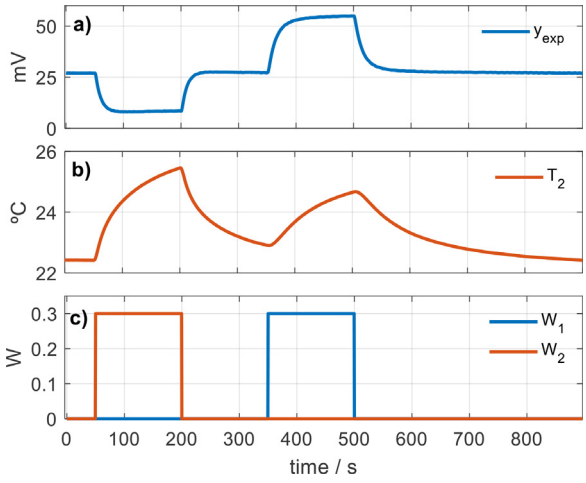

Fig. 2. Calibration measurement of the skin calorimeter: (a) Calorimetric signal y_{exp}, (b) Thermostat temperature T_2, (c) Base (W_1 in blue) and thermostat (W_2 in red) powers.

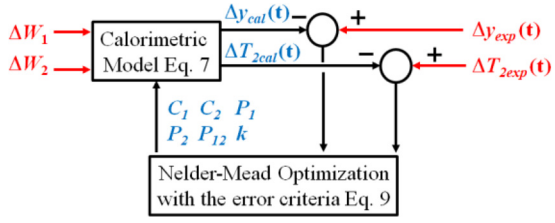

Fig. 3. Diagram of the calculation process used in the calorimeter calibration. The experimental input curves are shown in red and the parameters to be determined and the calculated curves are shown in blue.

$$+\frac{1}{np}\sqrt{\sum_{i=1}^{np}\left(\Delta T_{2\,\mathrm{exp}}[i]-\Delta T_{2cal}[i]\right)^2} \tag{9}$$

…where, np is the number of points used in the adjustment (np = 1800 in Fig. 2) and α is the weight of the calorimetric signal error. For ΔT_2 in °C and Δy in volts, α = 100. The relationship between the temperatures and the calorimetric signal is given by the Seebeck coefficient ($k \approx 20$ mV/K, its inverse 50 K/V). Experimentally we observe that, in steady state and for a constant thermostat temperature, the oscillations of the calorimetric signal are ± 0.2 mV, and the oscillations of the thermostat temperature are ± 10 mK. With α=100 in the error criterion, we give double weight to the calorimetric signal error over the error of the thermostat temperature. Since this is a simplified model of the experimental reality, it is difficult to completely and simultaneously fit both curves, and we have considered this compromise solution that gives an RMSE of 12.2 μV for the calorimetric signal and 1.3 mK for the thermostat temperature. The calculation process used in the calibration of the skin calorimeter is shown in Fig. 3. The results of the identification are given in Table 1 and Fig. 4 shows the fit between the experimental curves and those calculated with the model.

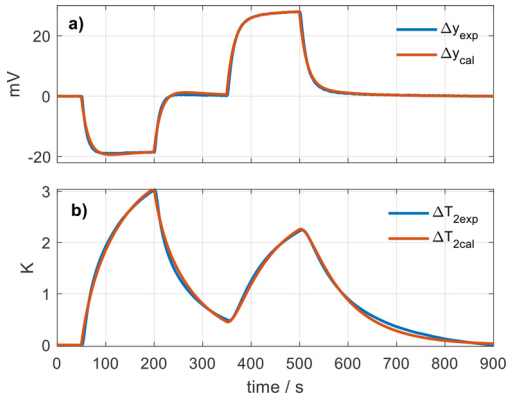

Fig. 4. Fit between experimental (*exp* in blue) and calculated (*cal* in red) curves: a) Calorimetric signal Δy, b) Thermostat temperature ΔT_2.

This modelization has two advantages:

- Although the proposed model is a major simplification of the experimental reality, it relates accurately the input signals (powers W_1 and W_2) with the output signals (thermostat temperature and calorimetric signal). This is shown by the good fit between the experimental curves and those calculated by the model (Fig. 4).
- The model parameters are directly related with the physical reality of the instrument as they adequately represent the heat capacities of the calibration base and thermostat domains.

2.4. Determination of heat capacity and equivalent thermal resistance of the skin

To determine the thermal properties of the skin, it is necessary to cause a thermal perturbation on the skin to study its static and dynamic response. This is done by programming a variation of the thermostat temperature when the calorimeter is applied to the skin (Fig. 5).

The proposed *skin calorimeter – skin* model is the same used in the calorimeter calibration, but in this case the first domain is the skin. The second domain is the calorimeter thermostat, connected by the thermal conductance P_{12} to the skin. We rewrite the model equation keeping the subscript 2 for the thermostat:

$$\Delta W_{skin}(t)=\frac{C_{skin}}{k}\frac{d\Delta y}{dt}+\frac{P_{skin}+P_{12}}{k}\Delta y+C_{skin}\frac{d\Delta T_2}{dt}+P_{skin}\Delta T_2 \tag{10}$$

The measurement procedure consists of placing the calorimeter on the skin with an adaptable holder (Fig. 5). First, the thermo-

Fig. 5. Placement of the calorimeter on the volar area of the wrist.

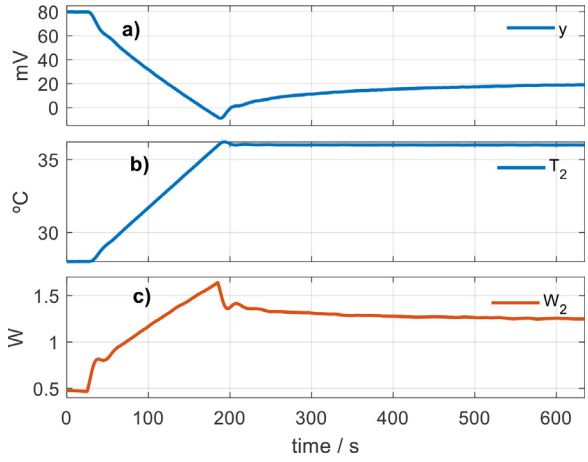

Fig. 6. A standard measurement procedure to determine the thermal properties of the skin. (a) Calorimetric signal y. (b) Thermostat temperature T_2. (c) Thermostat power W_2.

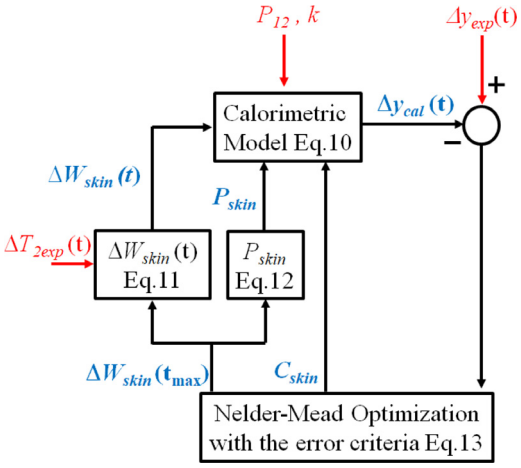

Fig. 7. Determination of the thermal properties of the skin. Input data are shown in red, and output data in blue.

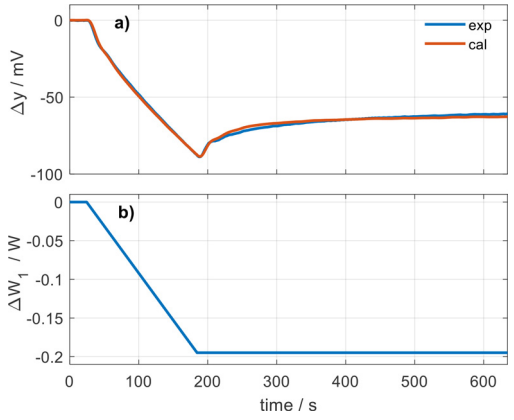

Fig. 8. (a) Fit of the experimental and calculated calorimetric signal ($\varepsilon_y = 33.3\ \mu$V), (b) Calculated skin power (ΔW_{skin}).

stat is programmed at a constant temperature. When the steady state is reached, a linear variation of the thermostat temperature is programmed, and the new temperature is maintained until the new steady state is reached. Fig. 6 shows the experimental curves of this type of measurement: calorimetric signal, temperature and thermostat power. In this case, the initial temperature of the thermostat is 28 °C and the final temperature is 36 °C, with a linear temperature variation rate of 3 K/min. This measurement was performed on the volar area of the left wrist of a healthy 64-year-old male subject.

When the calorimeter is applied on the skin, the human body is dissipating a power that we use as a reference. The difficulty is that when the thermostat's temperature increases, the heat power transmitted by conduction from the skin to the thermostat of the calorimeter decreases. With different measurements made with the thermostat at constant temperature [23] we have found that this relationship is linear. Therefore, we will assume that ΔW_{skin} (t) has the same form as ΔT_2 (t) but with the opposite sign.

$$\Delta W_{skin}(t) = -\Delta T_2 \left| \frac{\Delta W_{skin}(t_{\max})}{\Delta T_2(t_{\max})} \right| \tag{11}$$

The increments ΔW_{skin} (t_{max}) and ΔT_2 (t_{max}), are the values of these curves for the final time (t_{max}) or steady state. For this steady state, we define an equivalent thermal resistance of the skin with Eq. (12), where ΔT_2 (t_{max}) is the total temperature variation of the thermostat and P_{12} is the conductance between the skin surface and the thermostat (see Table 1).

$$R_{skin} = \frac{1}{P_{skin}} = \left| \frac{\Delta T_2(t_{\max})}{\Delta W_{skin}(t_{\max})} \right| - \frac{1}{P_{12}} \tag{12}$$

Two hypotheses are considered in the calculation process. The first one consists of considering that the power transmitted by conduction from the skin to the calorimeter has the same shape as the programmed temperature of the thermostat Eq. (11). The second one consists of defining a thermal resistance of the skin given by Eq. (12), which is obtained in the steady state.

The calculation method is shown in Fig. 7. The input data are the model parameters determined in the calibration of the calorimeter (P_{12} and k) and the experimental curves y (t) and T_2 (t). With the initial estimated values of C_{skin}, P_{skin} and ΔW_{skin} (t_{max}), the calorimetric response is determined with the model equation Eq. (10). The RMSE Eq. (13) is calculated and with an optimization method based on the Nelder–Mead simplex algorithm [20–22], the new values of C_{skin}, P_{skin} and ΔW_{skin} (t_{max}) are determined to construct ΔW_{skin} (t) and re-determine the calorimetric response and the new error. The process is repeated until the error criteria is minimized.

$$\varepsilon_y = \frac{1}{np}\sqrt{\sum_{i=1}^{np} (\Delta y_{\exp}[i] - \Delta y_{cal}[i])^2} \tag{13}$$

The fitting between the calculated and the experimental calorimetric signal is shown in Fig. 8. The RMSE is $\varepsilon_y = 33.3\ \mu$V for

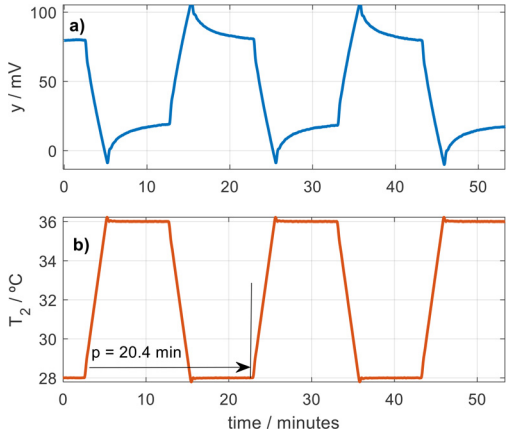

Fig. 9. Periodic measurement performed on the volar area of the left wrist of a healthy 64-year-old male subject. (a) calorimetric signal (y), (b) thermostat temperature (T_2).

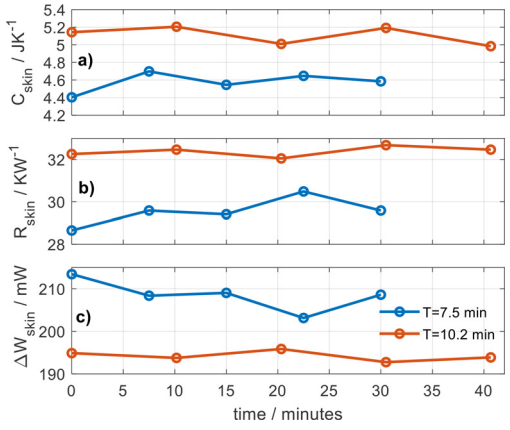

Fig. 10. Measured skin heat capacity and thermal resistance as a function of time in a periodic measurement of the type shown in Fig. 9 for two different periods. The skin heat flux variation is also plotted.

np = 1270 points used in the calculation. The power ΔW_{skin} (t) is also plotted, where ΔW_{skin} (t_{max}) = −195 mW. The resulting thermal properties are C_{skin} = 5.14 J/K and P_{skin} = 0.031 W/K (R_{skin} = 32.3 K/W).

This method is of great interest, so we programmed continuous measurements to determine the heat capacity and the thermal resistance of the skin as a function of time. In this way, we could monitor these thermal properties. For this purpose, periodical measurements with consecutive heating and cooling were programmed, as shown in Fig. 9. In the case shown, the period is p = 20.4 min.

Using the described method, the parameters C_{skin}, P_{skin} and ΔW_{skin} were determined for the case shown in Fig. 9 (p = 20.4 min) and for another equivalent case but with a shorter period of p = 15 min. Fig. 10 shows the results for both cases. We can see that when the period increases, the value of the heat capacity determined is greater. For p = 15 min, C_{skin} is 4.6 J/K, and for p = 20.4 min, is 5.1 J/K (mean values).

Similarly, for the measured thermal resistance, its value increases with time: for p = 15 min R_{skin} = 1/ P_{skin} = 29.5 K/W, and for p = 20.4 min, R_{skin} = 1/ P_{skin} = 32.4 K/W (mean values). This suggests that the thermal penetration depth increases over time, so a specific study is necessary. We also note that the higher the resistance, the lower the heat flux, for R_{skin} = 29.5 K/W, ΔW_{skin} (t_{max}) = 208.5 mW, and for R_{skin} = 32.4 K/W, ΔW_{skin} (t_{max}) = 194.2 mW. This is expected.

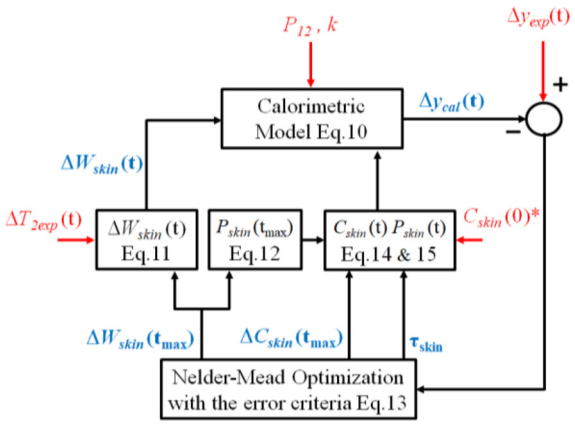

Fig. 11. Process to determine the thermal properties of the skin in the time - variant consideration. Inputs are shown in red and outputs in blue. C_{skin} (0) * is obtained in a previous fitting.

3. Results of the experimental study of the thermal probing depth

In Section 2.4 we verified that the measured heat capacity and thermal resistance of the skin increase with time. The skin region affected and measured increases with the time of exposure to the temperature change. Recent studies confirm similar results. In a recent work, dynamic thermal phenomena are studied in the SiGe HBT transistors when excited by sinusoidal power dissipation. This study introduces the concept of thermal penetration depth and concludes that decreasing frequency increases the thermal penetration depth [24]. Another study by Gustafsson [25] proposes that the thermal probing depth is proportional to the square root of the exposure time.

In the calculations of Section 2.4, C_{skin} has been assumed to be constant, but now a time function for C_{skin} must be proposed. We have studied different functions, obtaining the best fits with the hypothesis of an exponential variation of C_{skin} of the form:

$$C_{skin}(t) = C_{skin}(0) + \Delta C_{skin}\frac{1-\exp(-t/\tau_{skin})}{1-\exp(-t_{\max}/\tau_{skin})} \tag{14}$$

In this expression C_{skin} (0) is the initial heat capacity of the skin, ΔC_{skin} is the increase of the heat capacity over the measurement time t_{max}, and the time constant of the exponential is τ_{skin}. As the exposure time increases, the thermal depth increases, and therefore the amount of mass and thus the measured heat capacity C_{skin} increases. As a consequence, P_{skin} decreases. In the calculation process we will assume that the measured thermal resistance R_{skin} (inverse of P_{skin}) increases in the same proportion as C_{skin} increases and with the same time constant Eq. (15). On the other hand, the steady state resistance (for $t = t_{max}$), will obey Eq. (12).

$$R_{skin}(0) = R_{skin}(t_{\max})\frac{C_{skin}(0)}{C_{skin}(t_{\max})}$$

$$R_{skin}(t) = \frac{1}{P_{skin}(t)} = R_{skin}(0) + \Delta R_{skin}\frac{1-\exp(-t/\tau_{skin})}{1-\exp(-t_{\max}/\tau_{skin})} \tag{15}$$

At this point, the calculation process is more complex Fig. 11). From the initial values of ΔW_{skin} (t_{max}), C_{skin} and τ_{skin}, we determine W_{skin} (t) with Eq. (11), P_{skin} (t_{max}) with Eq. (12) and C_{skin} (t) & P_{skin} (t) with Eqs. (14) and (15). With the model equation Eq. (10), the calorimetric signal is determined. Then, is compared with the experimental curve and the RMSE is determined Eq. (13). The Nelder-Mean algorithm determines the new values of ΔW_{skin} (t_{max}), C_{skin} and τ_{skin}. The process is repeated until the error criteria is minimized.

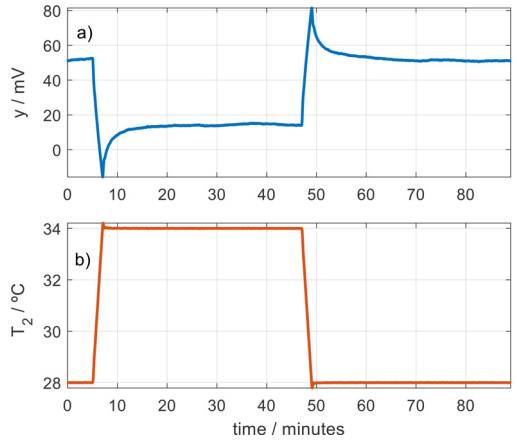

Fig. 12. Long duration measurement performed on the dorsal area of the dorsal area of the left wrist of a healthy 64-year-old male. (a) calorimetric signal (y), (b) thermostat temperature (T_2). T_{room} = 20.15 °C.

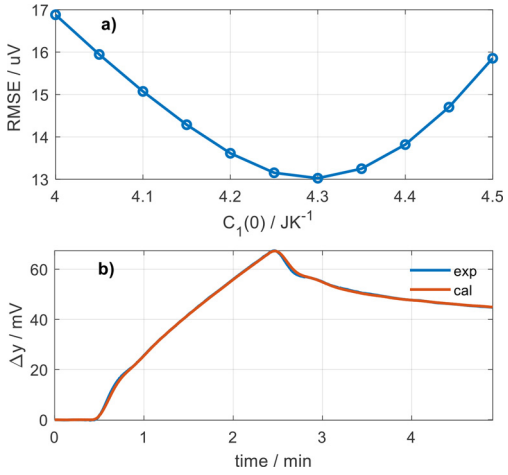

Fig. 13. Determination of the initial value of C_{skin} for the cooling case of the experimental measurement in Fig. 12. (a) RMSE for each value of C_{skin} (0) used in the calculation, (b) fit between the experimental and calculated calorimetric curve.

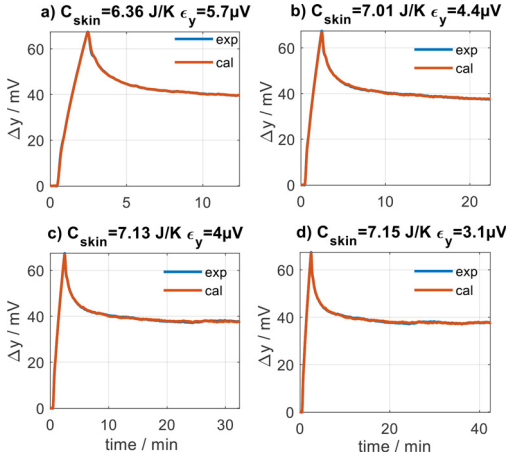

Fig. 14. Final value of C_{skin} and RMSE (ε_y) for the cooling case of the experimental measurement in Fig. 12. Calorimetric signal fittings for different times (t_{max}) used in the calculation. In all cases C_{skin} (0) = 4.3 J/K.

As an example of application we analyze the measurement shown in Fig. 6 where the thermostat temperature increase is 8 K. Proposing an exponential variation of C_{skin} Eq. (14) the RMSE of the calorimetric signal fit decreases to ε_y = 8.6 μV. In the invariant hypothesis we obtained an error ε_y = 33.3 μV (see Fig. 8). Now, the final measured heat capacity and thermal resistance of the skin are 6.23 J/K and 34.7 K/W. As expected, the value of C_{skin} obtained in the invariant hypothesis (5.14 J/K) is between the initial and final values of the variable hypothesis (between 4.40 and 6.23 J/K). Next, we study the measurement of these properties as a function of thermal perturbation exposure time. This study is performed on the dorsal and volar areas of the left wrist of a healthy 64-year-old male subject. We have found that the amplitude of the thermostat temperature increases and its change rate doesn't affect the results of the obtained values of measured heat capacity and thermal resistance. However, they affect the signal-to-noise ratio: the higher the amplitude and the speed, the higher the signal-to-noise ratio. The steady state noises are ± 0.2 mV for the calorimetric signal and ± 5 mK for the thermostat temperature. For a thermostat temperature change of 8 K at a rate of 3 K/min, the signal to noise ratios are: 592.5 (55.5 dB) for the calorimetric signal, 1600 (64.1 dB) for the thermostat temperature.

To study the thermal penetration depth, long-term measurements have been programmed. Fig. 12 shows the curves of one of the measurements used in this study. This measurement was performed on the dorsal area of the left wrist. The initial temperature of the thermostat was 28 °C and when it reached the steady state, an increase of 6 °C in 2 min (3 K/min) was programmed. The new temperature was maintained for 40 min and then we programmed it to return to the initial temperature with at the same rate. This measurement allows to obtain the values of the skin thermal properties as a function of time for heating and cooling cases.

An accurate calculation involves determining first the initial heat capacity C_{skin} (0) of Eq. (14). For this purpose, the initial zone of the curves corresponding to the temperature change of the thermostat is used. In the example shown, we take the first five minutes. Different values of C_{skin} (0) are proposed, and the iterative calculation program which scheme is shown in Fig. 11 is run. The value of C_{skin} (0) which gives the smallest error between the experimental and model-calculated curve is chosen. Fig. 13a shows the RMSE for each value of C_{skin} (0) used in the calculation (from 4 to 4.5 J/K). The lowest error is obtained for C_{skin} (0) = 4.3 J/K. Fig. 13b shows the calorimetric signal fitting for this case. For C_{skin} (0) = 4.3 J/K, C_{skin} (t_{max}) = 5.20 J/K and a RMSE of 13 μV. The case represented corresponds to the decrease of the thermostat temperature, which results in an increase of the power W_{skin} and the calorimetric signal.

Once the initial value of C_{skin} has been determined, the final values of C_{skin} and R_{skin} are calculated according to the procedure established in the diagram in Fig. 11. For this purpose, the experimental measurement is processed in sections: from the instant at which the temperature change begins up to a value t_{max}. Fig. 14 shows four steps of this process, in which the fit between the experimental and the calculated calorimetric curve is represented. In each case, the final value obtained for C_{skin} and the RMSE in the fit are indicated.

Now, we present the final results of this experimental study. Figs. 15 and 16 show the final values of the measured heat capacity and thermal resistance of the dorsal and volar area of the left wrist of the subject analyzed. The values obtained in the area of the curve corresponding to heating are shown in red, and the values obtained during cooling are shown in blue. Green line shows the exponential fit and Table 2 the parameters of the fit.

To conclude the results presentation, Fig. 17 shows the variation of the heat flux transmitted by conduction from the skin to the calorimeter in the case of an increase or decrease of 6 °C in the

Table 2
Measured heat capacity and thermal resistance of dorsal & volar wrist areas of a healthy 64-year-old male subject.

	C_{skin} (0) J/K	ΔC_{skin} J/K	τ_{skin} min	R_{skin} (0) K/W	ΔR_{skin} K/W	τ_{skin} min
Dorsal	4.10	2.93	6.1	32.9	11.7	5.8
Volar	4.00	3.00	6.9	27.2	8.5	6.5

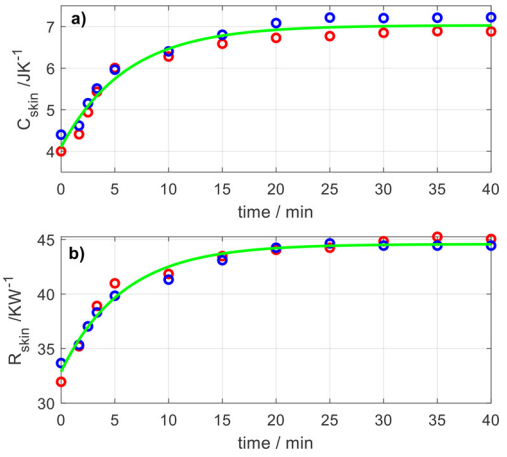

Fig. 15. Dorsal area of the left wrist of a healthy 64-year-old male subject. (a) Final values of measured skin heat capacity, (b) thermal resistance. Heating sections (red circles) and cooling ones (blue circles), exponential fit (green line).

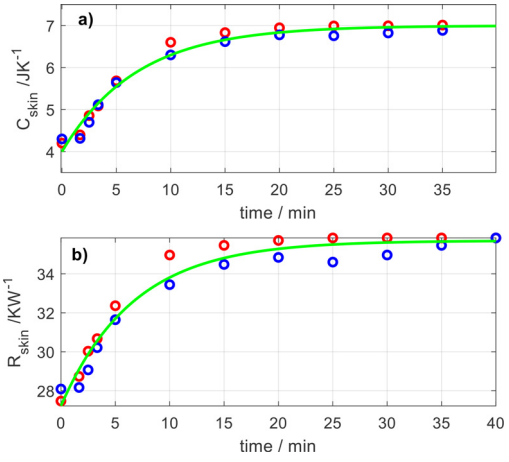

Fig. 16. Volar area of the left wrist of a healthy 64-year-old male subject. (a) Final values of measured skin heat capacity, (b) thermal resistance. Heating sections (red circles) and cooling ones (blue circles), exponential fit (green line).

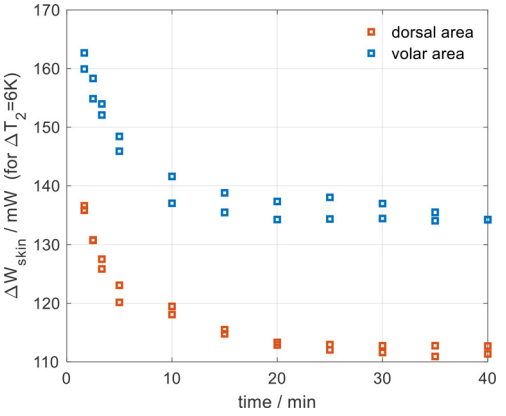

Fig. 17. Variation of the heat flux transmitted by conduction from the skin as a function of time for a 6 K increase or decrease of the thermostat temperature in the dorsal and volar areas of the wrist.

thermostat temperature. The graph clearly shows the stabilization of the skin affected by the thermal perturbation applied to it. It can also be seen how the volar zone has a greater dissipation as it has a lower measured thermal resistance.

4. Final discussion & conclusions

We developed a skin calorimeter to analyze a localized 4 cm^2 human skin region. The purpose of the device is to determine the heat flux, the heat capacity and the thermal resistance of that skin region. A simple two-body model is able to acceptably represent the operation of the calorimeter. The first element represents the skin region where the calorimeter is applied, and the second element represents the thermostat of the calorimeter.

To measure skin thermal magnitudes *in vivo*, a thermal excitation is required: the skin's response to this excitation will depend on its thermal properties. In our case, the excitation consists of a periodic temperature change while the calorimeter is applied on the skin.

Heat capacity measured with the skin calorimeter increases over time after the thermal excitation. Heat capacity determined is directly related with the volume of skin affected by the thermal excitation, and therefore with the depth of this volume, which we call thermal probing depth. In this work, we performed an experimental study of the thermal probing depth of the calorimeter. The results show that the thermal probing depth increases with the time after the thermostat temperature variation in an exponential trend, instead of a square root function.

To obtain these results, we used two different hypotheses. The first one considers invariant values of the measured heat capacity and thermal resistance. Then, a value between the initial and final value is obtained for the measurement period considered. This approach is useful since it allows to obtain quickly and easily average values of these magnitudes, but associated to a specific thermal penetration. In the second hypothesis, we consider that the measured heat capacity grows over time, and the measured thermal resistance increases at the same rate. This time – variant model considers the thermal properties as time functions. With this assumption we obtained a very acceptable fit of the calorimetric signal.

The measured skin thermal magnitudes depend on this thermal probing depth, hence the interest of this studies. Furthermore, study of the thermal probing depth allows thermal scanning of the analyzed skin region.

Measured heat capacity of the volar and dorsal areas of the wrist are of the same order of magnitude. From all the experimental data, we have an initial value of 4 J/K that increases, up to a final value of 7 J/K. This work is not aimed to quantify the depth of thermal measurement in millimeters. The skin is composed of different layers with slightly different thermal properties and a micrometric study would be required. The main objective is to show that the *in vivo* determination of the average heat capacity of the skin is a function of the time of exposure to the temperature change. We call this concept the thermal measurement depth. As a guideline, we indicate the thermal measurement depth in millimeters, for the case of considering an average specific heat capacity of the skin of 3391 $Jkg^{-1}K^{-1}$ and an average density of 1109 kgm^{-3} [26]. If we consider this average specific heat capacity of the skin,

and a detection surface of 4 cm^2, we have an initial thermal depth of 2.6 mm and a final depth of 4.6 mm, considering a prismatic homogeneous heat affected zone. If we consider an average specific heat capacity of the skin of 3.76 J/K cm^3 [26], and a detection surface of 4 cm^2, we have an initial thermal depth of 2.6 mm and a final depth of 4.6 mm, considering a prismatic homogeneous heat affected zone.

The measured thermal resistance of the dorsal area of the wrist is 25% higher than that of the volar area of the wrist. Therefore, the temperature of the volar zone is closer to the internal temperature. For this reason, as is well known, the volar area of the wrist is a good place to measure body temperature. In all results, both the measured heat capacity and the thermal resistance of the skin have an exponential time variation with time constants of the order of 6.5 min.

We emphasize the interest of monitoring the thermal properties of the skin by consecutive heating and cooling measurements such as those presented in this paper (Fig. 9). Monitoring of a skin pathology can be performed daily. Measurement of thermal resistance is of particular interest since it is very sensitive to the phenomena of sweating, vasoconstriction and vasodilation. We have performed preliminary measurements and have verified some of these relationships [13]. We consider that it is necessary to perform more measurements in humans, well designed in terms of scheduling, measurement time and type of activity.

This is a promising field of study. However, the dependence of the frequency of these periodic measurements on the penetration depth must always be taken into account. In this work, we highlight the relevance of considering the thermal penetration of the measurement. Therefore, it is proposed to perform the measurements with the same temperature schedule, so that the results are comparable. For the time constants of the prototype presented in this work, the period of periodical measurements can be reduced to 5 min, which is equivalent to a time of 2.5 min of exposure to temperature change. This time implies a thermal measurement depth that should be evaluated. On the other hand, the performed study allows to compare the results of the skin calorimeter with other instruments by taking as a meeting point the specific value of the heat capacity, directly related with the measurement thermal depth of each instrument.

Funding

This research did not receive any specific grant from funding agencies in the public, commercial, or not-for-profit sectors.

Declaration of Competing Interest

The authors declare that they have no known competing financial interests or personal relationships that could have appeared to influence the work reported in this paper.

CRediT authorship contribution statement

Pedro Jesús Rodríguez de Rivera: Conceptualization, Methodology, Validation, Investigation, Visualization. **Miriam Rodríguez de Rivera:** Validation, Data curation, Writing – original draft, Project administration. **Fabiola Socorro:** Validation, Resources, Supervision. **Manuel Rodríguez de Rivera:** Software, Conceptualization, Formal analysis, Writing – review & editing.

Data availability

Data will be made available on request.

References

[1] H.S. Carslaw, J.C. Jaeger, Conduction of Heat in Solids, Oxford at the Clarendon Press, London, 1959.
[2] E.H. Wissler, Pennes' 1948 paper revisited, J. Appl. Physiol. 85 (1) (1998) 35–41, doi:10.1152/jappl.1998.85.1.35.
[3] A. Lakhssass, E. Kengne, H. Semmaoui, Modifed Pennes' equation modeling bio-heat transfer in living tissues: analytical and numerical analysis, Nat. Sci. (Irvine) 2 (2010) 1375–1385, doi:10.4236/ns.2010.212168.
[4] Z.S. Deng, J. Liu, Blood perfusion-based model for characterizing the temperature fluctuation in living tissues, Phys. A 300 (3–4) (2001) 521–530, doi:10.1016/S0378-4371(01)00373-9.
[5] S. Hassanpour, A. Saboonchi, Modeling of heat transfer in a vascular tissue-like medium during an interstitial hyperthermia process, J. Therm. Biol. 62 (2016) 150–158, doi:10.1016/j.jtherbio.2016.06.022.
[6] M. Agrawal, K.R. Pardasani, Finite element model to study temperature distribution in skin and deep tissues of human limbs, J. Therm. Biol. 62 (2016) 98–105, doi:10.1016/j.jtherbio.2016.07.006.
[7] D. Sarkar, A. Haji-Sheikh, A. Jain, Temperature distribution in multi-layer skin tissue in presence of a tumor, Int. J. Heat Mass Transf. 91 (2015) 602–610, doi:10.1016/j.ijheatmasstransfer.2015.07.089.
[8] T. Okabe, T. Fujimura, J. Okajima, S. Aiba, S. Maruyama, Non-invasive measurement of effective thermal conductivity of human skin with a guard-heated thermistor probe, Int. J. Heat Mass Transf. 126 (2018) 625–635, doi:10.1016/j.ijheatmasstransfer.2018.06.039.
[9] N.M. Kharalkar, L.J. Hayes, J.W. Valvano, Pulse-power integrated-decay technique for the measurement of thermal conductivity, Measur. Sci. Technol. 19 (7) (2008) 075104, doi:10.1088/0957-0233/19/7/075104.
[10] R.M. Surabhi, Y. Ma, M. Patel, S. Krishnan, W. Chen, Y. Li, S. Xu, X. Feng, Y. Huang, A. John, Rogers epidermal electronic systems for measuring the thermal properties of human skin at depths of up to several millimeters, Adv. Funct. Mater. (2018) 1802083, doi:10.1002/adfm.201802083.
[11] A. Zubiaga, C. Kirsch, G. Boiger, M. Bonmarin, A simple instrument to measure the thermal transport properties of the human skin, in: Proceedings of the 2021 IEEE International Symposium on Medical Measurements and Applications (MeMeA), 2021, pp. 1–5, doi:10.1109/MeMeA52024.2021.9478754.
[12] X. Zhang, C. Bontozoglou, P. Xiao, *In vivo* skin characterizations by using opto-thermal depth-resolved detection spectra, Cosmetics 6 (2019) 54, doi:10.3390/cosmetics6030054.
[13] P.J.R. Rivera, M.R. Rivera, F. Socorro, J.A.L. Calbet, M.R. Rivera, Advantages of *in vivo* measurement of human skin thermal conductance using a calorimetric sensor, J. Therm. Anal. Calorim. 147 (2022) 10027–10036, doi:10.1007/s10973-022-11275-x.
[14] L. Yuan, J. Yu, S. Qian, Revisiting thermal penetration depth for caloric cooling system, Appl. Therm. Eng. 178 (2020) 115605, doi:10.1016/j.applthermaleng.2020.115605.
[15] P.J.R. Rivera, M.R. Rivera, F. Socorro, M.R. Rivera, *In vivo* measurement of skin heat capacity: advantages of the scanning calorimetric sensor, J. Therm. Anal. Calorim. 147 (2022) 12155–12163, doi:10.1007/s10973-022-11416-2.
[16] P.J.R. Rivera, M.R. Rivera, F. Socorro, M.R. Rivera, Heat flow measurement of human skin using a calorimetric sensor with a programmable thermostat. An alternative to climate chambers, Measurement 201 (2022) 1–10 111693, doi:10.1016/j.measurement.2022.111693.
[17] R. Kirchner, M. Rodríguez de Rivera, J. Seidel, et al., Identification of microscale calorimetric devices, J. Therm. Anal. Calorim. 82 (2005) 179–184, doi:10.1007/s10973-005-0861-9.
[18] C. Jesús, F. Socorro, M. Rodríguez de Rivera, New approach to Tian's equation applied to heat conduction and liquid injection calorimeters, J. Therm. Anal. Calorim. 110 (2012) 1523–1532, doi:10.1007/s10973-011-2117-1.
[19] P.J.R. Rivera, M.R. Rivera, F. Socorro, M.R. Rivera, Calibration and operation improvements of a calorimetric sensor for medical applications, Measurement 186 (2021) 1–12 110134, doi:10.1016/j.measurement.2021.110134.
[20] J.A. Nelder, C. Mead, A simplex method for function minimization, Comput. J. 7 (1965) 308–313, doi:10.1093/comjnl/7.4.308.
[21] J.C. Lagarias, J.A. Reeds, M.H. Wright, P.E. Wright, Convergence properties of the nelder–mead simplex method in low dimensions, SIAM J. Optim. 9 (1) (1998) 112–147 Vol.Number, doi:10.1137/S1052623496303470.
[22] Fun. Find minimum of unconstrained multivariable function using derivative-free method - MATLAB fminsearch - MathWorks España. (n.d.). Accesed November 22, 2022, from https://es.mathworks.com/help/matlab/ref/fminsearch.html
[23] P.J.R. Rivera, M.R. Rivera, F. Socorro, M.R. Rivera, Measurement of human body surface heat flux using a calorimetric sensor, J. Therm. Biol. 81 (2019) 178–184, doi:10.1016/j.jtherbio.2019.02.022.
[24] R. D'Esposito, S. Balanethiram, J.L. Battaglia, S. Frégonèse, T. Zimmer, Thermal penetration depth analysis and impact of the BEOL metals on the thermal impedance of SiGe HBTs, IEEE Electron. Device Lett. 38 (10) (2017) 1457–1460 Oct., doi:10.1109/LED.2017.2743043.
[25] S.E. Gustafsson, Transient plane source techniques for thermal conductivity and thermal diffusivity measurements of solid materials, Rev. Sci. Instrum. (1991), doi:10.1063/1.1142087.
[26] Hasgall PA, Di Gennaro F, Baumgartner C, Neufeld E, Lloyd B, Gosselin MC, Payne D, Klingenböck A, Kuster N, "IT'IS Database for thermal and electromagnetic parameters of biological tissues," Version 4.1, Feb 22, 2022, doi:10.13099/VIP21000-04-1.itis.swiss/database.